Calculation of differential cross section for dielectronic recombination with two-electron uranium

K. N. Lyashchenko[1,2,*] and O. Yu. Andreev[1]

[1]*Department of Physics, St. Petersburg State University, 7/9 Universitetskaya nab., St. Petersburg, 199034, Russia*

[2]*ITMO University, Kronverkskii ave. 49, 197101, Petergof, St. Petersburg, Russia*

(Received 24 February 2016; published 17 October 2016)

Calculation of the differential cross section for the dielectronic recombination with two-electron uranium within the framework of QED is presented. The polarization of the emitted photon is investigated. The contributions of the Breit interaction and the interference of the photon multipoles are studied. The Breit corrections to the widths of the energy levels are taken into account and are found to be very important for both the widths and the positions of the energy levels for three-electron ions.

DOI: 10.1103/PhysRevA.94.042513

I. INTRODUCTION

Dielectronic recombination with few-electron (in particular, with two-electron) highly charged ions is of interest both from experimental and theoretical points of view. Few-electron highly charged ions are relatively simple systems which allow precise theoretical description within the framework of quantum electrodynamics (QED). Dielectronic recombination is a resonant process where electron recombination with an ion is performed via formation of an autoionizing (doubly excited) state of the ion. Interelectron interaction plays a crucial role in formation of the doubly excited states. Accordingly, dielectronic recombination presents a tool for detailed investigation of dynamic electron correlations, in particular, for investigation of the Breit interaction.

Dielectronic recombination with two-electron ions of Fe was studied experimentally and theoretically in [1]. Measurements of the radiative and Auger decay rates for K-shell vacancies in highly charged Fe ions were presented in [2]. The linear polarization measurements of x rays emitted due to dielectronic recombination into highly charged Kr ions were recently presented in [3], and measurements of the dielectronic recombination resonant strengths of highly charged ions (in particular, two-electron Xe) were performed in [4]. Experimental investigation of dielectronic recombination with two- and three-electron ions of Pr, Ho, and Au is reported in [5]. In particular, dielectronic recombination strengths are measured and calculated. Experimental study of the dielectronic recombination with three-electron U ions is presented in [6]. Calculation of the transition rates for the doubly excited states of a three-electron ion of uranium was reported in [7]. The influence of the Breit and QED effects on the radiative transition parameters is analyzed in detail. Dielectronic recombination with two-electron uranium ion was also studied theoretically in [8]. In particular, the linear polarization and angular distribution of the x-ray photoemission was studied, and the contribution of the magnetic quadrupoles was investigated. Dielectronic recombination with one-electron uranium was studied experimentally and theoretically. The experimental study of the full cross section was performed in [9]. The corresponding calculations of the dielectronic recombination are presented in [9–13]. The electron recombination with highly charged ions presents a tool for investigation of the Breit interaction. The recent studies listed above showed that the Breit interaction may give important and even dominant contribution to the cross section of the dielectronic recombination with few-electron highly charged ions [9,13–18].

We consider the process of electron recombination with two-electron uranium initially being in its ground state. The final state is a three-electron ion in the ground state or in one of the singly excited states (r): $(1s1s2s)$ or $(1s1s2p)$. The first emitted photon (γ) can be registered in the experiment. If the energy of the initial state is close to the energy of a doubly excited state, the cross section shows resonances. The resonances are explained by the dielectronic recombination which can be written as

$$e^- + U^{90+}(1s1s) \to U^{89+}(d) \to U^{89+}(r) + \gamma \to \cdots , \tag{1}$$

where d is a doubly excited state: $(1s2s2s)$, $(1s2s2p)$, or $(1s2p2p)$. The considered process of electron recombination includes also the radiative electron capture (REC) [19] which is a nonresonant subprocess.

To study the cross section of the dielectronic recombination with highly charged ions, the QED calculations of the radiative transitions amplitudes between three-electron configurations are necessary. Such calculations can be performed with employment of various methods [12,20–24]. Within the framework of these methods both the resonant and nonresonant parts of the process of electron recombination are considered together and they cannot be separated unambiguously [12]. In the present paper the line-profile approach was used [23].

We present calculations of the full and differential cross sections for the dielectronic recombination with two-electron uranium within the framework of QED. The polarization of the emitted photon is investigated. The contributions of the Breit interaction and the interference of the photon multipoles are studied. At the end, we will estimate the contribution of the three-electron recombination for this collision system.

II. METHOD OF CALCULATION

The present calculations are based on the QED approach already applied for calculation of the cross section of electron recombination with one-electron ions [12,13]—the line-profile

*laywer92@mail.ru

approach (LPA) [23]. To describe the electron recombination with two-electron ions, the line-profile approach was generalized to three-electron systems. The incident electron is considered as an electron with certain momentum $\boldsymbol{p}$ and polarization μ and is described by the wave function $\psi_{\boldsymbol{p},\mu}$. Wave function ψ_{njlm} describes a bound electron with the corresponding quantum numbers [n, j, and m are the principle quantum number, total angular momentum, and its projection, respectively, and l defines the parity $(-1)^l$]. Employing expansion of the wave function $\psi_{\boldsymbol{p},\mu}$ in series over the wave functions of electron with certain energy ε, total angular momentum j, its projection m, and parity $(-1)^l$ the wave function of the incident electron can be written as [25]

$$\psi_{\boldsymbol{p},\mu}(\boldsymbol{r}) = \int d\varepsilon \sum_{jlm} a_{\boldsymbol{p}\mu,\varepsilon jlm}\psi_{\varepsilon jlm}(\boldsymbol{r}) \tag{2}$$

and

$$a_{\boldsymbol{p}\mu,\varepsilon jlm} = \frac{(2\pi)^{3/2}}{\sqrt{p\epsilon}} i^l e^{i\phi_{jl}} [\Omega^+_{jlm}(\boldsymbol{p}), \upsilon_\mu(\boldsymbol{p})]\delta(\epsilon - \varepsilon), \tag{3}$$

where $\Omega_{jlm}(\boldsymbol{p})$ is the spherical spinor, and $\upsilon_\mu(\boldsymbol{p})$ is the spinor with projection $\mu = \pm 1/2$ on the axis defined by electron momentum $\boldsymbol{p}$,

$$\left(\frac{\boldsymbol{p}}{|\boldsymbol{p}|}, \frac{\hat{\boldsymbol{\sigma}}}{2}\right)\upsilon_\mu(\boldsymbol{p}) = \mu\upsilon_\mu(\boldsymbol{p}), \tag{4}$$

where $\hat{\boldsymbol{\sigma}}$ is the Pauli vector, and the phase ϕ_{jl} is the Coulomb phase shift. Relativistic units are used throughout unless otherwise stated.

In the LPA the initial, final, and intermediate three-electron states are expanded in series of three-electron functions in the j-j coupling scheme. The following algorithm is employed for composition of the basis set of three-electron wave functions in the j-j coupling scheme. First, we select two electrons with closest energies and a composed two-electron wave function in the j-j coupling scheme

$$\Psi^{(0)}_{j_{12}m_{12}n_1j_1l_1n_2j_2l_2} = N \sum_{m_1m_2} \langle j_1m_1j_2m_2|J_{12}m_{12}\rangle \times \det\{\psi_{n_1j_1l_1m_1}, \psi_{n_2j_2l_2m_2}\}, \tag{5}$$

where N is a normalization constant (equal to $1/\sqrt{2}$ for nonequivalent electrons and $1/2$ for equivalent electrons) and $\langle j_1m_1j_2m_2|J_{12}m_{12}\rangle$ are Clebsch-Gordan coefficients. The electrons are represented by the quantum numbers n_i, j_i, l_i, and m_i (n_i denotes the principle quantum number for the bound electrons, and the energy for the electron from the continuum part of the spectrum j_i is the total angular momentum, l_i defines the parity, m_i is the projection of the total angular momentum, and $i = 1,2$ denotes the first and second electrons, respectively). Then we compose three-electron wave functions with certain angular momentum J and its projection M,

$$\Psi^{(0)}_{JMj_{12}n_1j_1l_1n_2j_2l_2n_3j_3l_3} = N \sum_{m_1m_2m_{12}m_3} \langle j_{12}m_{12}j_3m_3|JM\rangle \times \langle j_1m_1j_2m_2|j_{12}m_{12}\rangle \times \det\{\psi_{n_1j_1l_1m_1}, \psi_{n_2j_2l_2m_2}, \psi_{n_3j_3l_3m_3}\}, \tag{6}$$

where N is the normalization constant (equal to $1/\sqrt{12}$ for three-electron states with two equivalent electrons and to $1/\sqrt{6}$ for states without equivalent electrons). If three-electron configurations contain three equivalent electrons, the coefficients of fractional parentage $(j_1j_2[j_{12}]j_3J\|j_1j_2j_3\nu J)$ are to be calculated for composing the three-electron wave functions in the j-j coupling scheme [26–28]

$$\Psi^{(0)}_{JM\gamma n_1j_1l_1n_2j_2l_2n_3j_3l_3} = \sum_{j_{12}} (j_1j_2[j_{12}]j_3J\|j_1j_2j_3\nu J) \times \Psi^{(0)}_{JMj_{12}n_1j_1l_1n_2j_2l_2n_3j_3l_3}. \tag{7}$$

Here the quantum number ν denotes repeating terms of the electronic structure (if necessary).

The initial state of the system [a two-electron ion in its ground ($1s1s$) state and an incident electron] can be described by the wave function

$$\Psi^{\rm ini} = \frac{1}{\sqrt{6}} \det\{\psi_{n_1j_1l_1m_1}, \psi_{n_2j_2l_2m_2}, \psi_{\boldsymbol{p},\mu}\}. \tag{8}$$

The wave function $\psi_{\boldsymbol{p},\mu}$ describes the incident electron with momentum $\boldsymbol{p}$ and polarization μ, the wave function ψ_{njlm} describes a bound electron with the corresponding quantum numbers n, j, l, and m. Employing the expansion of Eq. (2) the wave function of the initial state can be presented as a linear combination of the following determinants:

$$\Psi^{(0)}_{n_1j_1l_1m_1n_2j_2l_2m_2\varepsilon j_3l_3m_3} = \frac{1}{\sqrt{6}} \det\{\psi_{n_1j_1l_1m_1}, \psi_{n_2j_2l_2m_2}, \psi_{\varepsilon j_3l_3m_3}\}. \tag{9}$$

Accordingly, the wave function of the initial state can be expanded into a series of three-electron functions with certain total momentum (in the j-j coupling scheme)

$$\Psi^{\rm ini} = \sum_{JMj_{12}n_1j_1l_1n_2j_2l_2j_3l_3} \int d\varepsilon \, \langle \Psi^{(0)}_{JMj_{12}n_1j_1l_1n_2j_2l_2\varepsilon j_3l_3} | \, \Psi^{\rm ini}\rangle \times \Psi^{(0)}_{JMj_{12}n_1j_1l_1n_2j_2l_2\varepsilon j_3l_3}. \tag{10}$$

The final state [($1s1s2s$), ($1s1s2p$) three-electron states] can be written as a three-electron configuration in the j-j coupling scheme

$$\Psi^{\rm fin} = \Psi^{(0)}_{JMj_{12}n_1j_1l_1n_2j_2l_2n_3j_3l_3}. \tag{11}$$

To describe highly charged ions within the framework of QED, the LPA was employed [12,23]. The interaction with the quantized electromagnetic and electron-positron fields leads to interelectron interaction, electron self-energy, and vacuum polarization corrections to the amplitude. Within the LPA the system is considered to be enclosed in a sphere of a large radius $R \to \infty$. Then, the incident electron can be described by a normalized wave function which corresponds to an artificial bound electron state (e_R). For calculation of the amplitudes of the transitions between bound states the standard QED perturbation theory for the quasidegenerate states can be applied [21,23,29,30].

Within the LPA we introduce g, the set of three-electron configurations which includes all the three-electron configurations composed by $1s,2s,2p,3s,3p,3d$ electrons and the electron e_R describing the incident electron. There is also

introduced the matrix V which is defined by the one and two-photon exchange, electron self-energy, and vacuum polarization matrix elements. Matrix $V = V^{(0)} + \Delta V$ is considered as a block matrix

$$V = \begin{bmatrix} V_{11} & V_{12} \\ V_{21} & V_{22} \end{bmatrix} = \begin{bmatrix} V_{11}^{(0)} + \Delta V_{11} & \Delta V_{12} \\ \Delta V_{21} & V_{22}^{(0)} + \Delta V_{22} \end{bmatrix}. \tag{12}$$

Matrix V_{11} is defined on set g, which contains configurations mixing with the reference state $n_g \in g$. Matrix $V^{(0)}$ is a diagonal matrix, its diagonal elements give energies of the three-electron configurations without regard to the interaction with the quantized fields which are the sum of the one-electron Dirac energies of the corresponding electrons. Matrix ΔV_{11} is not a diagonal matrix, but it contains a small parameter of the QED perturbation theory. Matrix V_{11} is a finite-dimensional matrix and can be diagonalized numerically. Then, the standard perturbation theory can be applied for the diagonalization of the matrix V.

The amplitude of the electron recombination is written as a matrix element of the photon emission operator $\Xi^{(0)}$ with the bra and ket vectors given by the eigenfunctions of the matrix V: $\Psi^{\rm fin}$ and $\Psi^{\rm ini}$ corresponding to the final and initial states of the system, respectively, with

$$U_{if} = \langle \Psi^{\rm fin} | \Xi | \Psi^{\rm ini} \rangle. \tag{13}$$

The operator Ξ is derived within the QED perturbation theory order by order [12,23]. The operator Ξ can be represented by its matrix elements, in the zeroth order of the perturbation theory it reads

$$\Xi^{(0)}_{u_1u_2u_3d_1d_2d_3} = eA^{(k,\lambda)*}_{u_1d_1}\delta_{u_2d_2}\delta_{u_3d_3} + \delta_{u_1d_1}eA^{(k,\lambda)*}_{u_2d_2}\delta_{u_3d_3} + \delta_{u_1d_1}\delta_{u_2d_2}eA^{(k,\lambda)*}_{u_3d_3}, \tag{14}$$

where $u_1, u_2, u_3, d_1, d_2, d_3$ are one-electron states with certain total angular momentum and parity, and the one-electron matrix elements $A^{(k,\lambda)*}_{ud}$ are defined as

$$A^{(k,\lambda)*}_{ud} = \int d^3\boldsymbol{r}\, \overline{\psi}_u(\boldsymbol{r})\gamma^\nu A^{(k,\lambda)*}_\nu(\boldsymbol{r})\psi_d(\boldsymbol{r}), \tag{15}$$

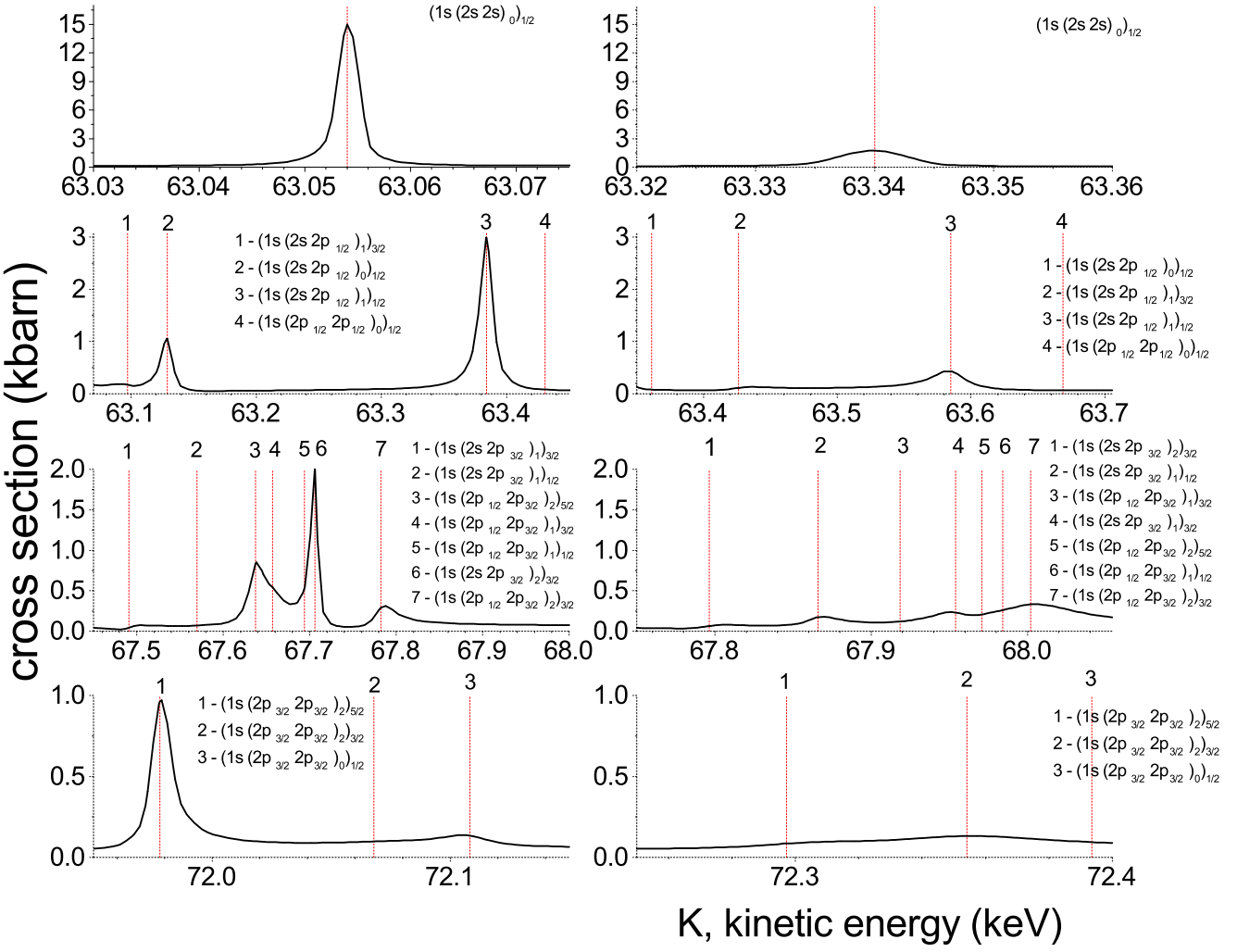

FIG. 1. The total cross section of the dielectronic recombination with two-electron uranium as a function of the kinetic energy of the incident electron K. The left column correspond to full QED calculation (Coulomb + Breit with retardation) and the right column denote the calculation with disregard of the Breit interaction. Red dashed vertical lines indicate the positions of the resonances with the doubly excited states.

TABLE I. Comparison of the energies ($E - 3mc^2 = \Delta E - i\frac{\Gamma}{2}$, in keV) of three electronic states and corresponding resonance kinetic energies (ϵ) of the impact electron (on the second line for each state). Second and third columns show the diagonal element of the matrix V [see Eq. (12)]. Columns 4–6 show eigenvalues of the matrix V with different electron-electron interaction models.

"	V Coulomb		V Coulomb+Breit (with retardation)		Coulomb		Coulomb+Breit (without retardation)		Coulomb+Breit (with retardation)	
Three electron	ΔE	Γ	ΔE	Γ	ΔE	Γ	ΔE	Γ	ΔE	Γ
state	ϵ		ϵ		ϵ		ϵ		ϵ	
$[1s(2s\,2s)_0]_{1/2}$	−198.350	0.000	−198.304	0.000	−198.377	0.004	−198.327	0.004	−198.332	0.002
	63.366		63.078		63.340		63.058		63.054	
$[1s(2s\,2p_{1/2})_1]_{3/2}$	−198.282	0.031	−198.281	0.021	−198.291	0.031	−198.281	0.031	−198.289	0.021
	63.433		63.102		63.426		63.105		63.097	
$[1s(2s\,2p_{1/2})_0]_{1/2}$	−198.299	0.032	−198.231	0.016	−198.357	0.032	−198.245	0.032	−198.256	0.011
	63.416		63.151		63.360		63.140		63.129	
$[1s(2s\,2p_{1/2})_1]_{1/2}$	−198.174	0.032	−198.009	0.006	−198.131	0.032	−198.000	0.032	−198.002	0.012
	63.541		63.373		63.585		63.385		63.384	
$[1s(2p_{1/2}\,2p_{1/2})_0]_{1/2}$	−198.058	0.063	−197.962	0.032	−198.048	0.059	−197.944	0.060	−197.954	0.031
	63.658		63.421		63.669		63.441		63.431	
$[1s(2s\,2p_{3/2})_1]_{3/2}$	−193.832	0.027	−193.795	0.003	−193.769	0.027	−193.679	0.027	−193.901	0.026
	67.883		67.588		67.948		67.706		67.485	
$[1s(2s\,2p_{3/2})_1]_{1/2}$	−193.856	0.026	−193.821	0.034	−193.857	0.026	−193.824	0.026	−193.822	0.034
	67.859		67.561		67.860		67.561		67.563	
$[1s(2p_{1/2}\,2p_{3/2})_2]_{5/2}$	−193.745	0.058	−193.747	0.022	−193.750	0.058	−193.730	0.058	−193.752	0.022
	67.970		67.635		67.967		67.655		67.634	
$[1s(2p_{1/2}\,2p_{3/2})_1]_{3/2}$	−193.788	0.058	−193.717	0.016	−193.801	0.058	−193.718	0.058	−193.732	0.029
	67.928		67.665		67.915		67.667		67.654	
$[1s(2p_{1/2}\,2p_{3/2})_1]_{1/2}$	−193.732	0.057	−193.690	0.056	−193.736	0.057	−193.698	0.057	−193.695	0.056
	67.983		67.692		67.980		67.687		67.691	
$[1s(2s\,2p_{3/2})_2]_{3/2}$	−193.860	0.026	−193.788	0.032	−193.927	0.026	−193.897	0.026	−193.686	0.009
	67.855		67.594		67.790		67.488		67.700	
$[1s(2p_{1/2}\,2p_{3/2})_2]_{3/2}$	−193.723	0.058	−193.610	0.041	−193.717	0.058	−193.594	0.058	−193.606	0.029
	67.993		67.772		67.999		67.791		67.780	
$[1s(2p_{3/2}\,2p_{3/2})_2]_{5/2}$	−189.426	0.053	−189.415	0.010	−189.426	0.053	−189.385	0.053	−189.414	0.010
	72.289		71.968		72.291		72.001		71.971	
$[1s(2p_{3/2}\,2p_{3/2})_2]_{3/2}$	−189.369	0.052	−189.324	0.052	−189.369	0.052	−189.325	0.052	−189.324	0.052
	72.346		72.058		72.348		72.060		72.061	
$[1s(2p_{3/2}\,2p_{3/2})_0]_{1/2}$	−189.334	0.053	−189.288	0.027	−189.332	0.053	−189.269	0.053	−189.286	0.027
	72.381		72.094		72.385		72.117		72.100	

where γ^ν are Dirac gamma matrices. The emitted photon wave function is $A_\nu^{(k,\lambda)*} = (A_0^{(k,\lambda)*}, \boldsymbol{A}^{(k,\lambda)*})$. We use a gauge in which $A_0^{(k,\lambda)} = 0$. The vector part of the photon wave function $\boldsymbol{A}^{(k,\lambda)}$ reads as

$$\boldsymbol{A}^{(k,\lambda)}(\boldsymbol{r}) = \sqrt{\frac{2\pi}{\omega}} e^{i\boldsymbol{k}\boldsymbol{r}} \boldsymbol{e}^{(\lambda)}, \tag{16}$$

where ω and $\boldsymbol{k}$ are frequency and momentum of the photon, respectively. Employing the multipole expansion we can write [31]

$$\boldsymbol{A}^{(k,\lambda)} = \sqrt{\frac{2\pi}{\omega}} \sum_{j_0 l_0 m_0} i^{l_0} g_{l_0}(\omega r)[\boldsymbol{e}^{(\lambda)}, \boldsymbol{Y}^*_{j_0 l_0 m_0}(\boldsymbol{k})]\boldsymbol{Y}_{j_0 l_0 m_0}(\boldsymbol{r}), \tag{17}$$

where $g_{l_0}(x) = 4\pi j_{l_0}(x)$ and $j_{l_0}(x)$ is the spherical Bessel function, the $\boldsymbol{Y}_{j_0 l_0 m_0}$ are the vector spherical harmonics, and $\boldsymbol{e}^{(\lambda)}$ is the vector of photon polarization. We consider the linear polarizations of the photon

$$\boldsymbol{e}_1 = \frac{[\boldsymbol{p}\times\boldsymbol{k}]}{|[\boldsymbol{p}\times\boldsymbol{k}]|}, \quad \boldsymbol{e}_2 = \frac{[\boldsymbol{e}_1\times\boldsymbol{k}]}{|[\boldsymbol{e}_1\times\boldsymbol{k}]|} \tag{18}$$

and the circular polarizations of the photon

$$\boldsymbol{e}_+ = \frac{1}{\sqrt{2}}(\boldsymbol{e}_1 + i\boldsymbol{e}_2), \quad \boldsymbol{e}_- = \frac{1}{\sqrt{2}}(\boldsymbol{e}_1 - i\boldsymbol{e}_2). \tag{19}$$

The z axis is defined by the incident electron momentum $\boldsymbol{p}$. Accordingly, the vectors $\boldsymbol{p}$, $\boldsymbol{k}$ and the polarization vectors look like

$$\frac{\boldsymbol{p}}{|\boldsymbol{p}|} = \begin{pmatrix}0\\0\\1\end{pmatrix}, \quad \frac{\boldsymbol{k}}{|\boldsymbol{k}|} = \begin{pmatrix}\sin\theta\cos\phi\\ \sin\theta\sin\phi\\ \cos\theta\end{pmatrix}, \tag{20}$$

$$\boldsymbol{e}_1 = \begin{pmatrix}-\sin\phi\\ \cos\phi\\ 0\end{pmatrix}, \quad \text{and} \quad \boldsymbol{e}_2 = \begin{pmatrix}\cos\theta\cos\phi\\ \cos\theta\sin\phi\\ -\sin\theta\end{pmatrix}, \tag{21}$$

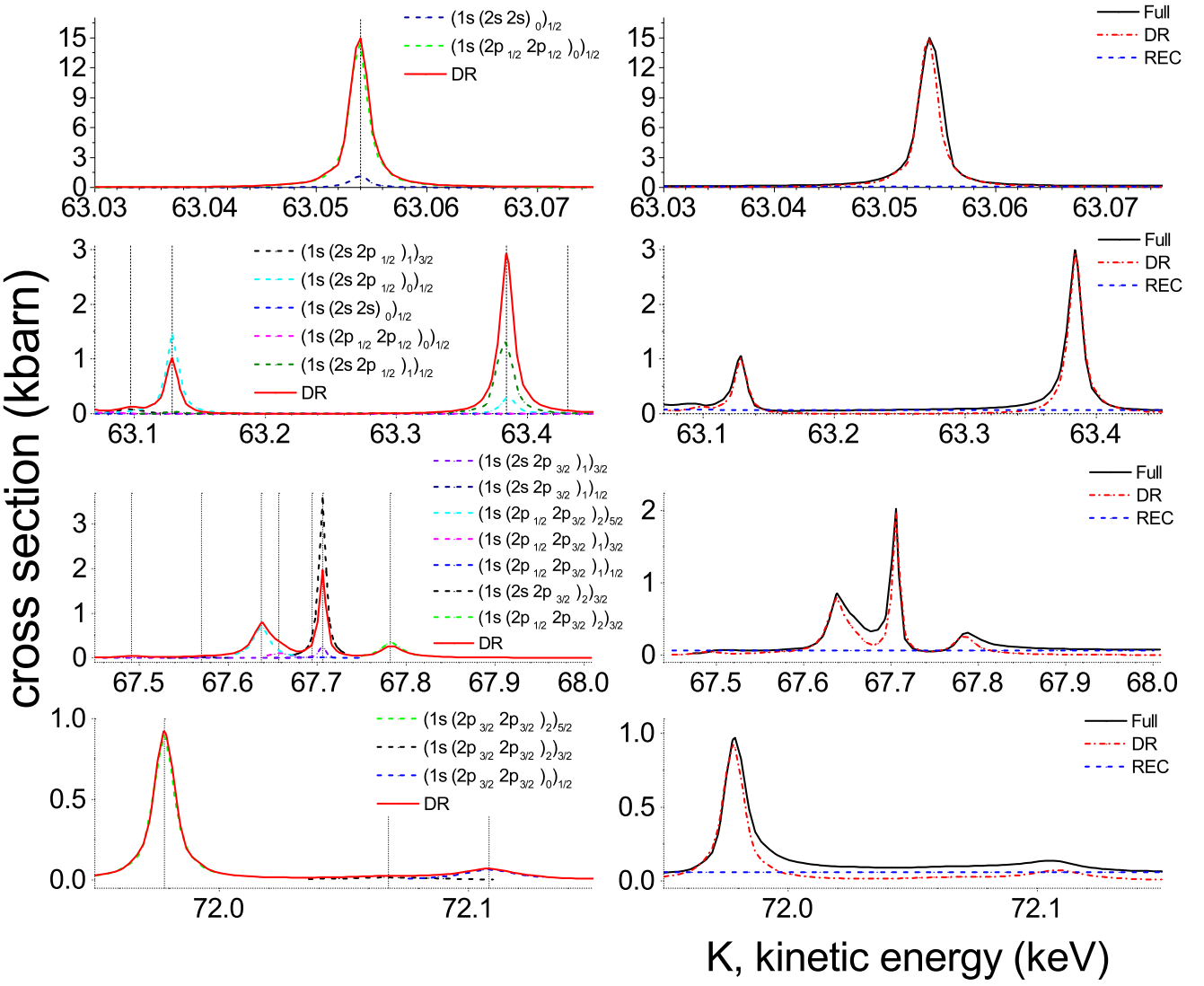

FIG. 2. Interference figures. The left column corresponds to the interference of the individual peaks with each other. The dashed curves represent the total cross section for the individual peaks (without REC). The red (dashed-dotted) curves represents the total cross section for dielectronic recombination (without REC). Vertical lines indicate the positions of the resonances with the doubly excited states. The right column corresponds to the interference of DR (red curves) and REC [blue (dashed) lines]. Black solid curves denotes the full calculation.

respectively. The electron-ion collision process has an axial symmetry and does not depend on the angle ϕ.

The operator Ξ in the first order of the perturbation theory gives a small contribution and is omitted in the present calculation.

III. RESULTS

We have studied the process of electron recombination with two-electron uranium being initially in its ground state. The process is considered in the rest frame of the uranium ion. We investigated regions of the incident electron energy where the role of dielectronic recombination is prominent, restricting ourselves to the consideration of four low lying energy regions, in particular, the regions where the energy of the initial state [$(1s1s)$ plus incident electron e] is close to the energies of doubly excited states $(1s2s2s)$, $(1s2s2p)$, $(1s2p2p)$. Accordingly, we performed the calculations for the following resonance regions of the incident electron (kinetic) energy: [63.03,63.075] keV, [63.075,63.45] keV, [67.25,68.00] keV, and [71.95,72.15] keV.

The total cross section of electron recombination with two-electron uranium is presented as a function of the kinetic energy of the incident electron in Fig. 1. The left four graphs represent the exact QED calculation of the total cross section for the four resonance regions, respectively. The right ones represent the calculation of the total cross section with disregard of the Breit interelectron interaction (in the Feynman graphs corresponding to the one- and more photon exchange). The graphs reveal a large contribution of the Breit interaction to the cross section.

We note that the relative contribution of the Breit interaction to the cross section for dielectronic recombination with two-electron uranium ions is much larger than that for dielectronic recombination with one-electron ions (see [9,13]). The importance of the Breit interaction is explained by large

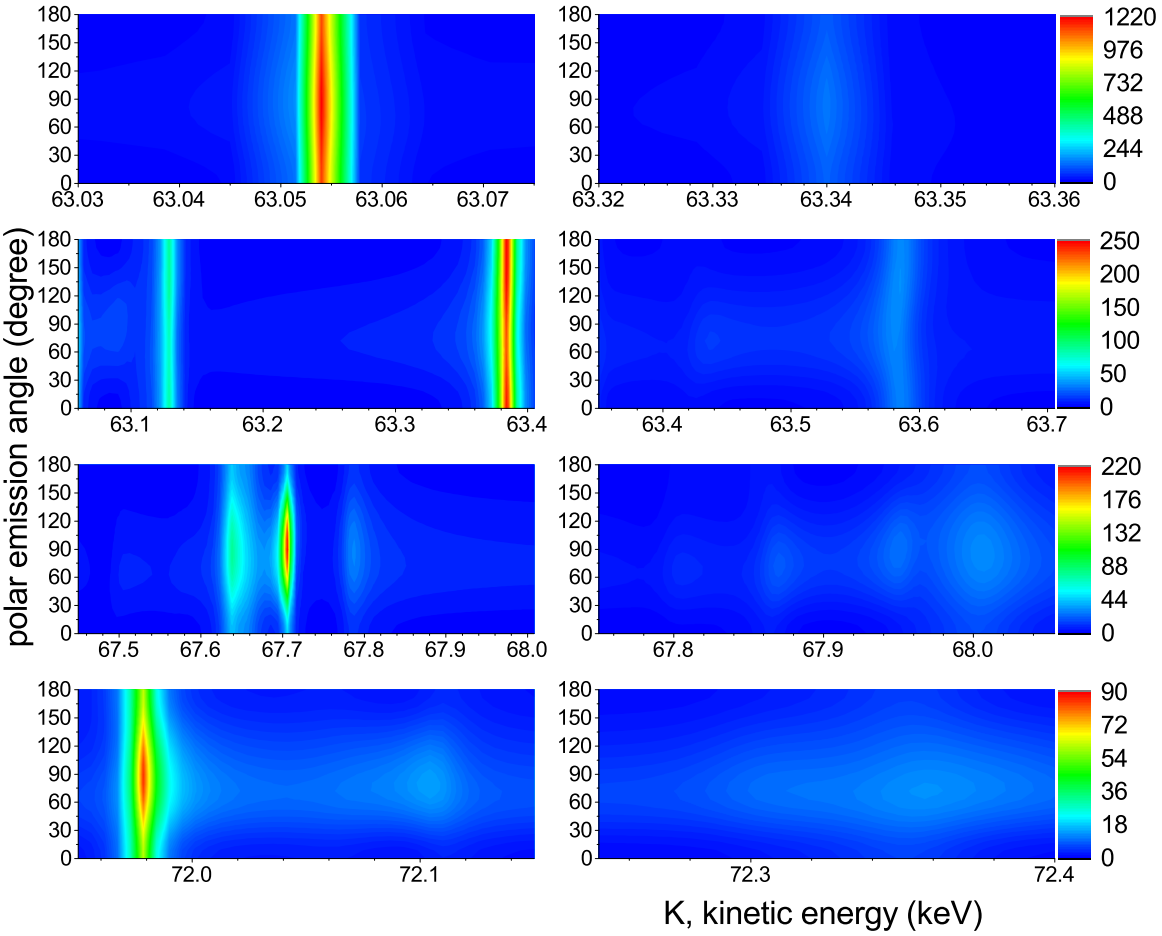

FIG. 3. The differential cross section ($d\sigma/d\Omega$, in barn/sr) of dielectronic recombination vs K. The graphs in the left column correspond to the full QED calculation (Coulomb + Breit with retardation) of the differential cross section, the graphs in the right column present the calculation with disregard of the Breit interaction.

sensitivity of the widths of three-electron energy levels to the Breit interaction. Within the framework of the standard QED theory, the energy shift of energy levels (due to the interaction with quantized electromagnetic and electron-positron fields) is commonly written as $\Delta E = \mathrm{Re}\{\Delta E\} - i\frac{\Gamma}{2}$ [21,23,29,32], where $\mathrm{Re}\{\Delta E\}$ is a correction to the energy, and Γ defines the width of the energy level. For the one- and two-electron configurations the major contribution to Γ is usually given by the electron self-energy Feynman graph. However, for three-electron configurations the contribution of the electron self-energy graph can be largely canceled by the contribution of the Breit part of the one-photon exchange graph. For example, $(1s1s2s)$ configuration is the ground state of a three-electron ion, so the contribution of the imaginary part of the electron self-energy graph is completely canceled by contribution of the Breit part of the one-photon exchange graph. It can be referred as a realization of the Pauli exclusion principle [31]. We note that in the case of the considered three-electron doubly excited states we take into account the interelectron interaction between the $1s$ electron and the excited L-shell electrons. However, it is not the case if we consider the dielectronic recombination with one-electron ions where the two-electron doubly excited states [such as $(2s,2s),(2s,2p),(2p,2p)$] do not contain the $1s$ electron. The retardation is more significant for the interaction of the electrons with larger energy difference, hence, the retardation should be more important for the dielectronic recombination with two-electron uranium ions.

The energies and widths of the doubly excited states considered are very sensitive to the Breit interaction. In Table I we present data which show the role of the Breit interaction for the doubly excited states. Doubly excited states are specified in the first column. In the second and the third columns (V Coulomb and V Coulomb+Breit) are values of the diagonal matrix elements of matrix V [see Eq. (12)]; these data are given by summation of the diagonal matrix elements of the corresponding Feynman graphs (electron self-energy, vacuum polarization, one-photon exchange, and part of the two-photon exchange graphs). The column V Coulomb+Breit contains results of the exact QED calculation, the column V Coulomb presents results of the calculation with disregard of the Breit part of photon exchange graphs. These data have no clear physical meaning, but they demonstrate a strong cancellation of the imaginary parts of the electron self-energy and the Breit part of the photon exchange corrections for some of the configurations. The next three columns present results of calculation of the energies and widths of the doubly excited states performed within the exact QED approach

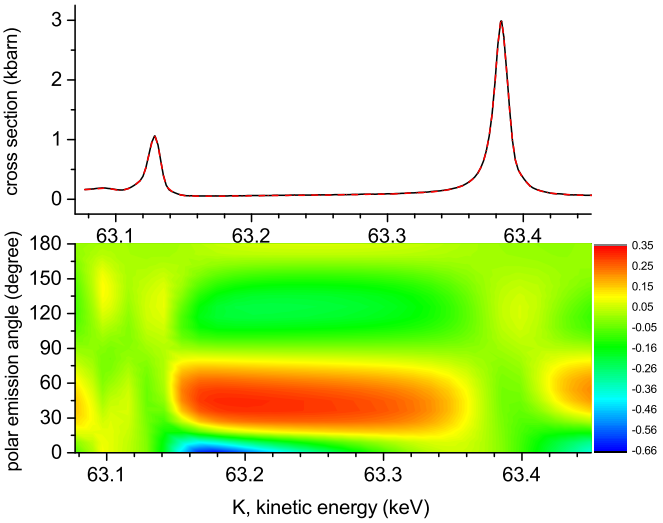

FIG. 4. The contribution of the higher multipoles to the full and differential cross sections. The top graph corresponds to the full cross section (in kbarn). Red dashed curve represent calculation where just $j_0 = 1$ [see Eq. (17)] taken into account. Black solid curve denotes the calculation with $0 < j_0 < 10$. The bottom graph represents the relative contribution of the higher multipoles $\delta\sigma$ [see Eq. (23)].

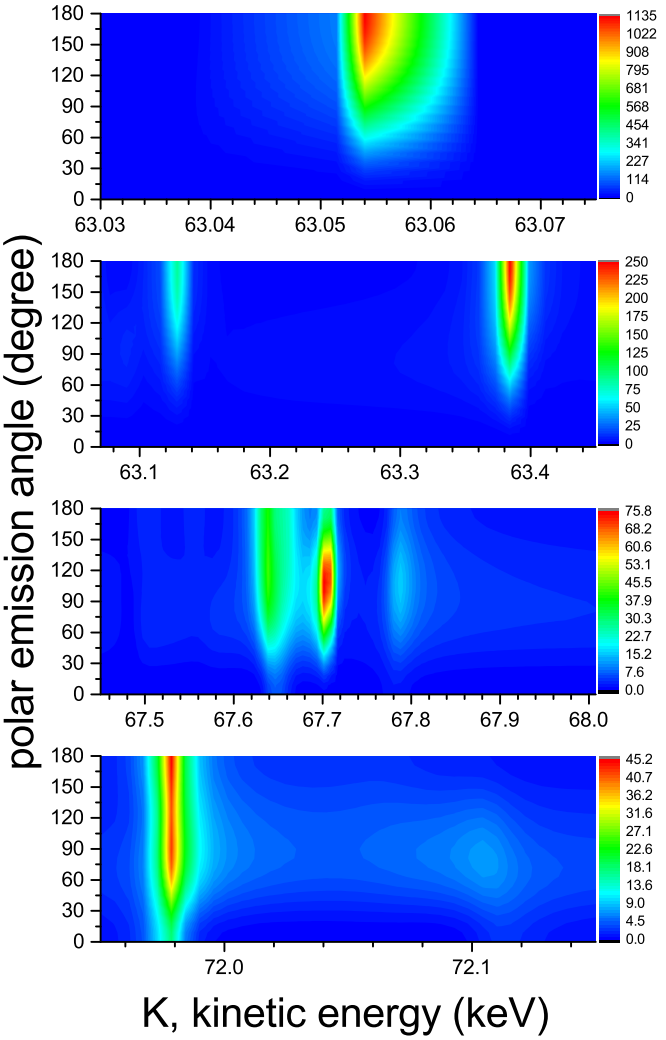

FIG. 5. The differential cross sections ($d\sigma/d\Omega$, in barn/sr) of dielectronic recombination with two-electron uranium for polarized incident electrons ($\mu = -1/2$) and the photon emission with circular polarization $\mathbf{e}_+$ [see Eq. (19)].

[column Coulomb+Breit (with retardation)], with disregard of retardation in the Breit interaction [column Coulomb+Breit (without retardation)] and with complete neglect of the Breit interaction (column Coulomb). The corresponding resonance kinetic energies of the incident electron are also given. These data demonstrate the importance of the Breit interaction for the energies and widths of the doubly excited states that explain the large contribution of the Breit interaction to the cross section for the dielectronic recombination with two-electron uranium ions seen in Fig. 1.

The process of dielectronic recombination proceeds via formation of doubly excited states, corresponding to peaks in their cross sections. In order to study the individual contributions of the doubly excited states, we performed calculations of the cross section where only fixed doubly excited states were taken into account. The results are presented in Fig. 2. Plots in the left column show individual contribution of the doubly excited states. Plots in the right column show the separate contribution of the resonant channel (electron capture via formation of doubly excited states, i.e., dielectronic recombination) and the nonresonant channel (REC). We note that partition of the electron recombination into resonant and nonresonant channels is ambiguous. Results of the full calculation of the cross section are given with a mark (Full) in Fig. 2. These plots also show interference between the dielectronic recombination and the radiative electron capture.

Results of calculation of the differential cross section (in barn/sr)

$$\sigma' \equiv d\sigma/d\Omega \tag{22}$$

as a function of the kinetic energy of incident electron K are given in Fig. 3. The left plots present the exact QED calculation, the right plots present results of calculation with disregard of the Breit interaction. As a consequence of large contribution of the Breit interaction to the total cross section (see Fig. 1), the Breit interaction is also important for the differential cross section of electron capture by two-electron uranium ion.

In the present calculation the multipole expansion of the emitted photon wave function was employed [see Eq. (17)]. The multipoles up to $j_0 = 9$ were taken into account. Investigation of the contribution of the higher multipoles of the emitted photon is presented in Fig. 4. The upper plot presents the total cross section. The red curve in the upper plot corresponds to calculation of the total cross section within the dipole approximation where only terms with $j_0 = 1$ are taken into account in the multipole expansion Eq. (17). The black curve in the upper plot corresponds to the full calculation ($j_0 \leqslant 9$). It is seen that contribution of the higher multipoles to the total cross section is insignificant. The lower plot shows the differential cross section: there is a relative difference between the differential cross section calculated in the dipole approximation $\sigma'^{(j_0=1)}$ and the full calculation σ'

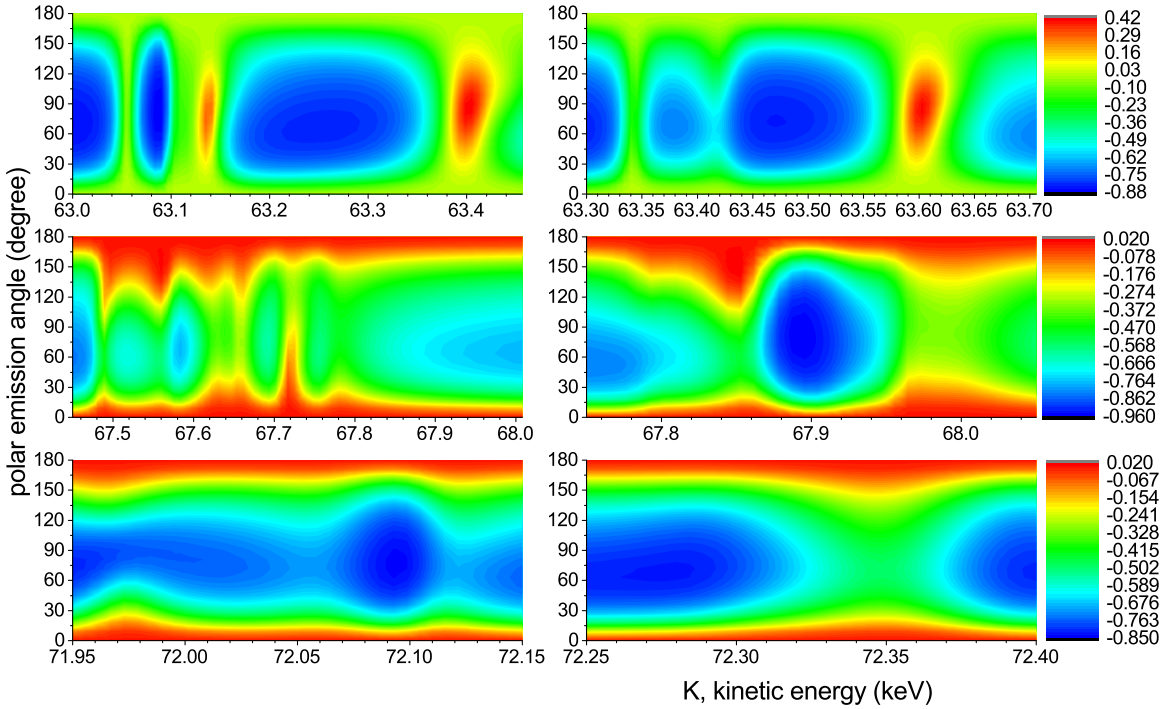

FIG. 6. The Stokes parameter P_1 [see Eq. (25)] vs K. The graphs in the left column correspond to the full QED calculation (Coulomb + Breit with retardation) of the differential cross section, the graphs in the right column present the calculation with disregard of the Breit interaction.

[see Eq. (22)]:

$$\delta\sigma = \frac{\sigma'^{(j_0=1)} - \sigma'}{\sigma'}. \tag{23}$$

In spite of a small contribution of the higher multipoles to the total cross section (<5%), they play a significant role for the differential cross section. Our calculations show that mainly due to the interference between $E1$, $M1$ and $E2$, $M2$ emitted

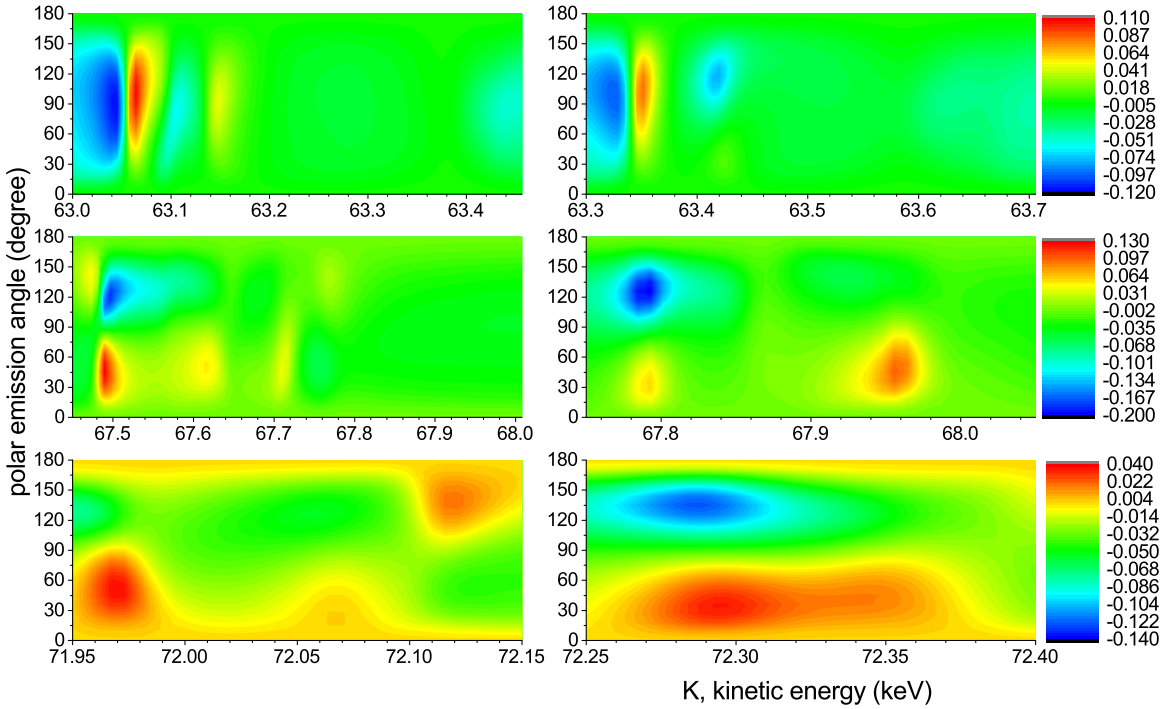

FIG. 7. The Stokes parameter P_2 [see Eq. (26)] vs K. The graphs in the left column correspond to the full QED calculation (Coulomb + Breit with retardation) of the differential cross section, the graphs in the right column present the calculation with disregard of the Breit interaction.

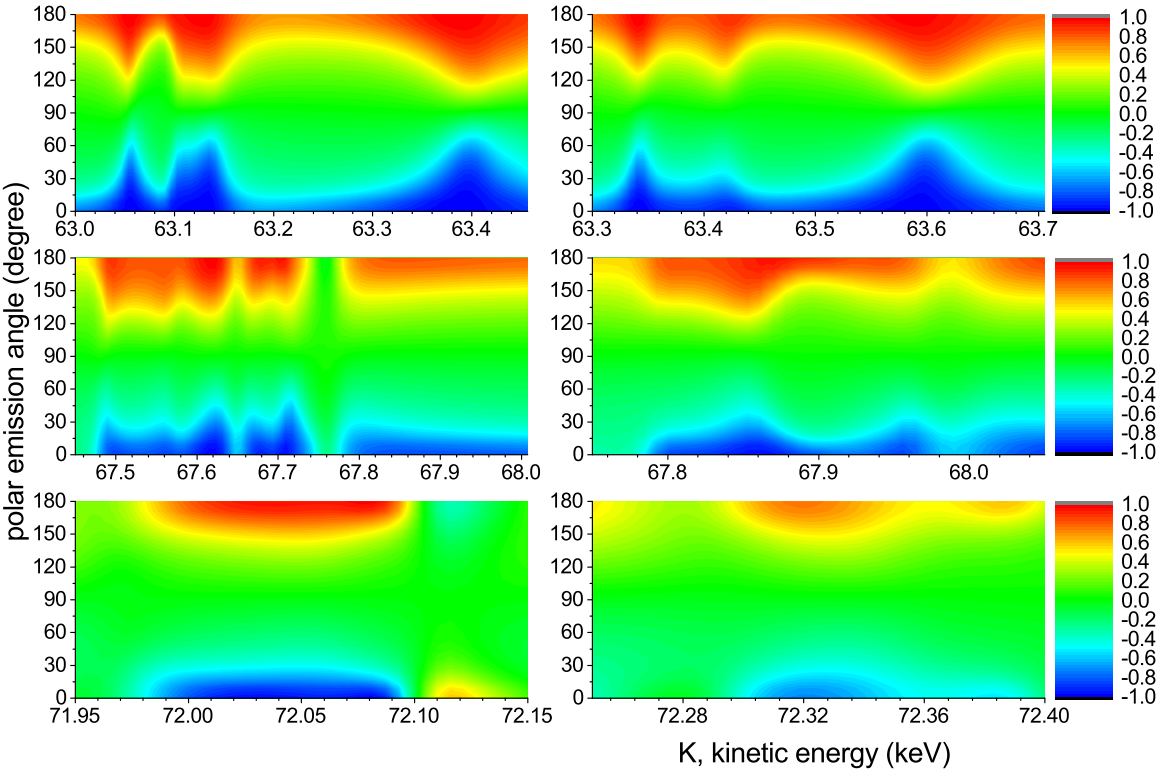

FIG. 8. The Stokes parameter P_3 [see Eq. (27)] vs K. The graphs in the left column correspond to the full QED calculation (Coulomb + Breit with retardation) of the differential cross section, the graphs in the right column present the calculation with disregard of the Breit interaction.

photons, $\delta\sigma$ may reach up to 66% in regions between the peaks.

We have also studied the contribution of the various polarizations of the incident electron and emitted photon. Polarization of the initial state is defined by polarization of the incident electron (projection of the spin onto the direction of momentum) which can be equal to $\mu = \pm 1/2$. Different polarizations of the incident electron give equal contributions to the cross section, while the summation over the photon polarizations is performed; however, they give different contributions if the polarization of the emitted photon is fixed. In Fig. 5 we present results of calculations of the differential cross section σ'_{-+}, where the incident electron has polarization $\mu = -1/2$ and the emitted photon has polarization $\boldsymbol{e}_+$ [see Eq. (19)]. The result of the calculation of the differential cross section σ'_{--} (the polarization of incident electron is $\mu = -1/2$, and the photon polarization is $\boldsymbol{e}_-$) can be obtained from Fig. 5 by inversion of the polar axis. Differential cross sections with different polarizations are connected by the following condition:

$$\sigma'_{\mu,-} = \sigma'_{-\mu,+}. \tag{24}$$

To investigate the polarizations of the emitted photon, we calculated the Stokes parameters. We have calculated the Stokes parameters for incident electrons with polarization $\mu = -1/2$; the results of the calculations are presented in Figs. 6–8. The Stokes parameters P_1 and P_2 for different linear polarizations of the photon are given in Figs. 6 and 7:

$$P_1 = \frac{\sigma'_{0^\circ} - \sigma'_{90^\circ}}{\sigma'_{0^\circ} + \sigma'_{90^\circ}}, \tag{25}$$

$$P_2 = \frac{\sigma'_{45^\circ} - \sigma'_{135^\circ}}{\sigma'_{45^\circ} + \sigma'_{135^\circ}}, \tag{26}$$

where σ'_{0°, σ'_{90° are the differential cross section for emission of the photon with its polarization vector in or orthogonal to the $(\boldsymbol{p},\boldsymbol{k})$ plane, respectively, and σ'_{45°, σ'_{135° are the differential cross sections for emission of the photon with the polarization vector at 45° and 135° to the $(\boldsymbol{p},\boldsymbol{k})$ plane, respectively. The Stokes parameters P_1 and P_2 are equal to zero at angles 0° and 180° [see Eq. (21)]. The Stokes parameter (P_3) describing the circular polarization Eq. (19) is presented in Fig. (8):

$$P_3 = \frac{\sigma'_+ - \sigma'_-}{\sigma'_+ + \sigma'_-}, \tag{27}$$

where $\sigma'_\pm \equiv d\sigma_\pm/d\Omega$ are the differential cross section for emission of the photon with the corresponding chirality. Figures 6–8 show that Stokes parameters also very sensitive to Breit interaction.

For unpolarized incident electrons the corresponding polarizations of the emitted photon give equal contributions to the differential cross sections σ'_{45°, σ'_{135°, and σ'_-, σ'_+, respectively. Accordingly, the Stokes parameters P_2 and P_3 are equal to zero. The parameter P_1 is independent of the polarization of the incident electron and is the same for the polarized and unpolarized incident electrons.

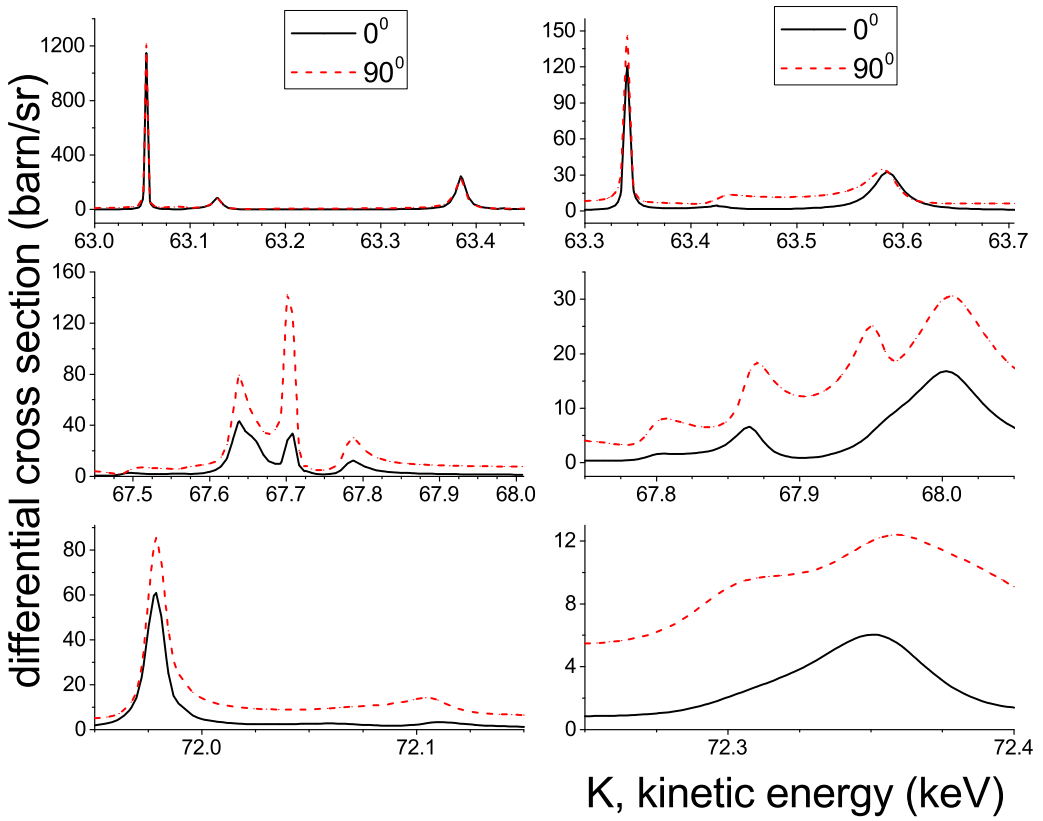

FIG. 9. The comparison of the differential cross section for photon emission at 0° angle [$\sigma'(\theta = 0°)$, black (solid) curve, in barn/sr] and the differential cross section for photon emission at 90° angle [$\sigma'(\theta = 90°)$, red (dashed) curve, in barn/sr]. The graphs in the left column correspond to the full QED calculation (Coulomb + Breit with retardation) of the differential cross section, the graphs in the right column present the calculation with disregard of the Breit interaction.

For addition characteristics of angular distribution we present the differential cross section with photon emission angles 0° [$\sigma'(\theta = 0°)$], 90° [$\sigma'(\theta = 90°)$] in Fig. 9 and the asymmetry parameter [18]

$$A = \frac{\sigma'(\theta = 90°)}{\sigma'(\theta = 0°)} \tag{28}$$

in Fig. 10, respectively. The calculations show that the emission to 90° dominates over emission to 0°, particularly in regions of the resonance energies. Far from the resonance regions the photon is emitted mainly at a 90° angle that results in corresponding growth of the parameter A. In the framework of the nonrelativistic approximation this phenomenon is naturally explained as a prohibition of the photon emission at 0° and 180° angles for REC with bare nuclei [19,33,34].

We would like to reiterate that we have also investigated the contribution of tri-electronic recombination to the process of electron capture by two-electron uranium ion initially being in its ground state. We performed calculations of the cross section for regions of the incident electron energy where the contribution of the triply excited states $[(2s2s)_0 2p_{1/2}]_{1/2}$ and $[(2p_{1/2}2p_{1/2})_0 2s]_{1/2}$ could be significant. It was found that the contributions of these states to the cross section is 8–11 orders smaller than the corresponding contribution of the (nonresonant) REC, and it offers no possibility to detect the tri-electronic recombination in experiment. However, we found that for the process of electron capture with two-electron uranium initially being in a single excited state [for example, $(1s2s)_0$], the contribution of the tri-electronic recombination is much larger than the corresponding contribution of the radiative electron capture, which, in principle, makes it possible to experimentally investigate the tri-electronic recombination.

In conclusion, we would like to list the main results obtained. We have presented QED calculations of the total cross sections of the dielectronic recombination with two-electron uranium ions initially being in their ground state. The results demonstrate the large contribution of the Breit interaction to the cross sections. In particular, the Breit corrections to the widths of the energy levels are taken into account and are found to be very important for both the widths and the positions of the energy levels. The interference between the resonant and nonresonant (REC) channels is investigated. The differential cross section for dielectronic recombination of unpolarized and polarized electrons with two-electron uranium ions is calculated. The results show that the differential cross section is very sensitive to the Breit interaction. We have also investigated the contribution of the higher multipoles of the photon wave-function expansion. It was found that their contributions to the differential cross sections are significant.

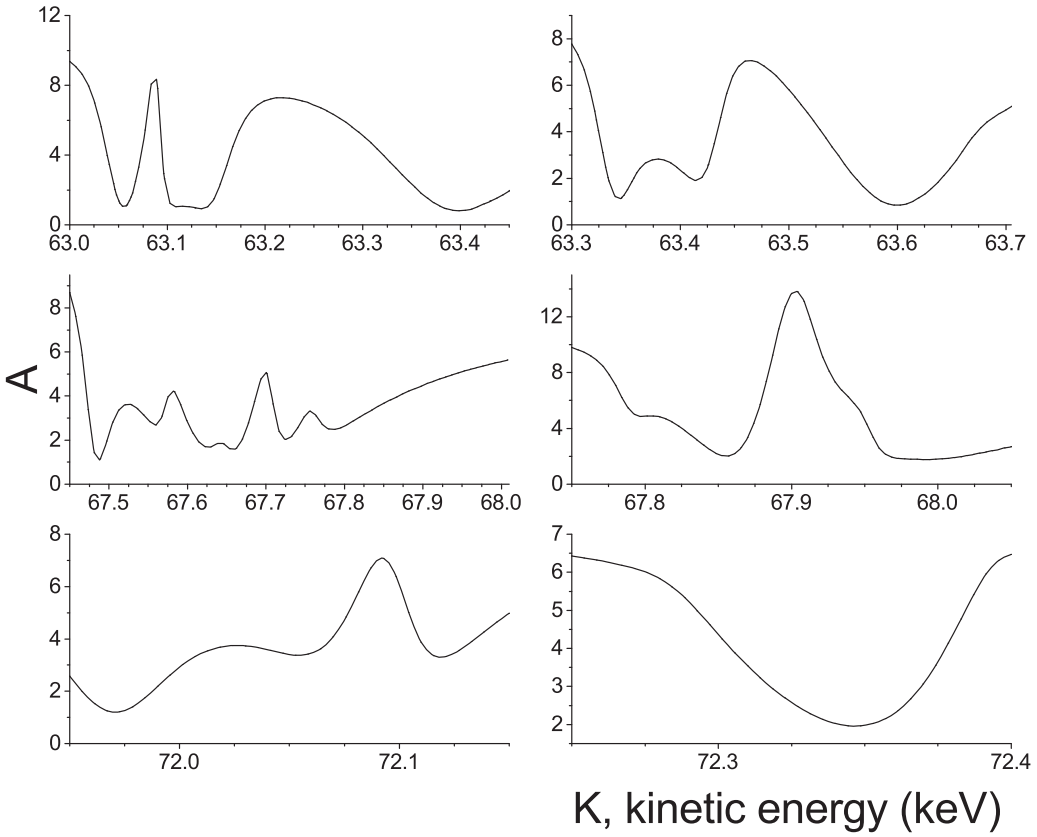

FIG. 10. The asymmetry parameter A [see Eq. (28)] is presented. The graphs in the left column correspond to the full QED calculation (Coulomb + Breit with retardation) of the differential cross section, the graphs in the right column present the calculation with disregard of the Breit interaction.

The polarization of the emitted photons and the photon emission asymmetry are investigated. The Stokes parameters and the symmetry parameter are calculated. The polarization parameters are very sensitive to the contributions of the Breit interaction. The role of the Breit interaction for the dielectronic recombination with two-electron uranium ions is very significant, which would allow one to perform a successful experimental investigation of the Breit interaction in the process of dielectronic recombination with two-electron uranium.

ACKNOWLEDGMENTS

The authors are indebted to senior lecturer V. V. Bankevich for reading and improving the manuscript. The authors acknowledge the support by RFBR Grant No. 14-02-20188. The work of K.N.L. was supported by RFBR Grant 16-32-00620, St. Petersburg State University through a research Grant 11.38.227.2014 and by the German-Russian Interdisciplinary Science Center (G-RISC, P-2016a-8) funded by the German Federal Foreign Office via the German Academic Exchange Service (DAAD).

[1] P. Beiersdorfer, T. W. Phillips, K. L. Wong, R. E. Marrs, and D. A. Vogel, Phys. Rev. A **46**, 3812 (1992).
[2] R. Steinbrügge, S. Bernitt, S. W. Epp, J. K. Rudolph, C. Beilmann, H. Bekker, S. Eberle, A. Müller, O. O. Versolato, H.-C. Wille *et al.*, Phys. Rev. A **91**, 032502 (2015).
[3] C. Shah, H. Jörg, S. Bernitt, S. Dobrodey, R. Steinbrügge, C. Beilmann, P. Amaro, Z. Hu, S. Weber, S. Fritzsche *et al.*, Phys. Rev. A **92**, 042702 (2015).
[4] K. Yao, Z. Geng, J. Xiao, Y. Yang, C. Chen, Y. Fu, D. Lu, R. Hutton, and Y. Zou, Phys. Rev. A **81**, 022714 (2010).
[5] Z. Hu, Y. Li, X. Han, D. Kato, X. Tong, H. Watanabe, and N. Nakamura, Phys. Rev. A **90**, 062702 (2014).
[6] S. Trotsenko, A. Gumberidze, Y. Gao, C. Kozhuharov, S. Fritzsche, H. F. Beyer, S. Hagmann, P.-M. Hillenbrand, N. Petridis, U. Spillmann *et al.*, Phys. Scr. **T166**, 014024 (2015).
[7] L. Natarajan, Phys. Rev. A **92**, 012507 (2015).
[8] Z. B. Chen, J. L. Zeng, H. W. Hu, and C. Z. Dong, J. Phys. B **48**, 144005 (2015).
[9] D. Bernhardt, C. Brandau, Z. Harman, C. Kozhuharov, A. Müller, W. Scheid, S. Schippers, E. W. Schmidt, D. Yu, A. N. Artemyev *et al.*, Phys. Rev. A **83**, 020701 (2011).
[10] V. V. Karasiov, L. N. Labzowsky, A. V. Nefiodov, and V. M. Shabaev, Phys. Lett. A **161**, 453 (1992).
[11] S. Zakowicz, W. Scheid, and N. Grün, J. Phys. B **37**, 131 (2004).

[12] O. Yu. Andreev, L. N. Labzowsky, and A. V. Prigorovsky, Phys. Rev. A **80**, 042514 (2009).
[13] K. N. Lyashchenko and O. Y. Andreev, Phys. Rev. A **91**, 012511 (2015).
[14] N. Nakamura, A. P. Kavanagh, H. Watanabe, H. A. Sakaue, Y. Li, D. Kato, F. J. Currell, and S. Ohtani, Phys. Rev. Lett. **100**, 073203 (2008).
[15] S. Fritzsche, A. Surzhykov, and T. Stöhlker, Phys. Rev. Lett. **103**, 113001 (2009).
[16] O. Matula, S. Fritzsche, F. J. Currell, and A. Surzhykov, Phys. Rev. A **84**, 052723 (2011).
[17] Z. Hu, X. Han, Y. Li, D. Kato, X. Tong, and N. Nakamura, Phys. Rev. Lett. **108**, 073002 (2012).
[18] C. Shah, P. Amaro, R. Steinbrügge, S. Bernitt, Z. Harman, S. Fritzsche, A. Surzhykov, J. R. C. López-Urrutia, and S. Tashenov, in 17th International Conference on the Physics of Highly Charged Ions (HCI 2014). Book of Abstracts, Bariloche, Argentina (2014), p. 174.
[19] J. Eichler, A. Ichihara, and T. Shirai, Phys. Rev. A **51**, 3027 (1995).
[20] W. R. Johnson, D. R. Plante, and J. Sapirstein, Adv. At. Mol. Opt. Phys. **35**, 255 (1995).
[21] V. M. Shabaev, Phys. Rep. **356**, 119 (2002).
[22] P. Indelicato, V. M. Shabaev, and A. V. Volotka, Phys. Rev. A **69**, 062506 (2004).
[23] O. Yu. Andreev, L. N. Labzowsky, G. Plunien, and D. A. Solovyev, Phys. Rep. **455**, 135 (2008).
[24] O. Yu. Andreev, L. N. Labzowsky, and G. Plunien, Phys. Rev. A **79**, 032515 (2009).
[25] A. I. Akhiezer and V. B. Berestetskii, *Quantum Electrodynamics* (Wiley Interscience, New York, 1965).
[26] G. Racah, Phys. Rev. **63**, 367 (1943).
[27] I. I. Sobelman, *Atomic Spectra and Radiative Transitions* (Springe, Berlin, 1979).
[28] M. G. Veselov and L. N. Labzowsky, *Teorija Atoma. Strojenie Elektronnykh Obolochek* [Theory of atoms. The Structure of the Electron Shells] (in Russian) (Nauka, Moscow, 1986).
[29] I. Lindgren, S. Salomonson, and B. Åsén, Phys. Rep. **389**, 161 (2004).
[30] I. Lindgren, S. Salomonson, and J. Holmberg, Phys. Rev. A **89**, 062504 (2014).
[31] L. Labzowsky, G. Klimchitskaya, and Yu. Dmitriev, *Relativistic Effects in the Spectra of Atomic Systems* (IOP, Bristol, 1993).
[32] F. Low, Phys. Rev. **88**, 53 (1952).
[33] M. Stobbe, Ann. Phys. (Leipzig) **7**, 661 (1930).
[34] H. Bethe and E. Salpeter, *Quantum Mechanics of One- and Two-Electron Atoms* (Academic, New York, 1957).